

Dislocation nucleation in the phase field crystal model

Vidar Skogvoll,¹ Audun Skaugen,² Luiza Angheluta,¹ and Jorge Viñals³

¹*PoreLab, The Njord Centre, Department of Physics,
University of Oslo, P. O. Box 1048, 0316 Oslo, Norway*

²*Helsinki Institute of Physics and Computational Physics Laboratory,
Tampere University, P.O. Box 692, FI-33014 Tampere, Finland*

³*School of Physics and Astronomy, University of Minnesota, Minneapolis, MN 55455*

We use the phase field crystal model to study the nucleation of edge dislocations under an applied stress field. Under quasi-static loading of a perfect lattice, a dislocation dipole nucleates (due to Burgers vector conservation) with Burgers vector and slip plane chosen according to the lattice orientation with respect to the applied stress. The phase field crystal correctly accounts for elastic energy storage prior to nucleation, and for dissipative relaxation during the nucleation event. We show that both a lattice incompatibility field and the resolved stresses are sensitive diagnostics of the fluctuations prior to nucleation, of the location of the nucleation event, and of the Burgers vector and slip direction of the dislocations that will be nucleated upon further increases in the stress. A direct calculation of the phase field energy accurately correlates with the nucleation event as signaled by the lattice incompatibility field. We finally show that a Schmid-like criterion predicts the critical nucleation stress.

Unlike the spontaneous and thermal nucleation of topological defects in a symmetry-breaking phase transition [1–3], the formation of dislocation lines in a material is typically studied as an athermal process largely driven by local stresses [4]. Since the existence and mobility of such defects are essential contributors to the strength and ductility of crystalline materials, understanding the mechanisms behind their creation and motion is a fundamental goal of materials science in general, and of plasticity theory in particular. Along parallel developments in the continuum theory of crystal plasticity, a number of empirical criteria have been introduced to predict dislocation nucleation thresholds, the resulting Burgers vector distribution, and line direction [5–8]. These macroscopic criteria have been extensively compared with microscopic results from Molecular Dynamics (MD) simulations of model crystalline solids in a variety of configurations and imposed stresses [8–11]. However, the details of the mechanical conditions that lead to dislocation nucleation still remain poorly understood, with criteria and numerical simulations often yielding conflicting phenomenology. The two main reasons why a precise comparison between the two is difficult include the disparity in length scales between crystal plasticity theory and simulation, and the necessity in the latter to thermally average phase space trajectories that take place over characteristic energy scales which are much higher than thermal scales. We bridge both sets of studies here by introducing a phase field crystal model [12, 13] of dislocation nucleation, and show that the nucleation event is well captured at the mesoscale by a continuum lattice incompatibility field. Our numerical results indicate that the nucleation event is governed by a local balance between the resolved stresses along lattice slip planes and the force acting between the nucleating dislocation pair, and that the incompatibility field predicts the Burgers vector of the nucleating defect pair. The simplest class of nucleation criteria rely on the so called Schmid stress

[5, 7, 14–17]. When an appropriate projection of an atomic level shear stress exceeds a material dependent threshold, a dislocation loop will be nucleated. While fcc crystals generally obey the resulting law, there exists an entire class on “non-Schmid” lattices [18]. For example, a recent, careful MD study of nucleation in a nanoindentation configuration for a model Lennard-Jones solid shows that the Schmid criterion not only fails to account for the site of the nucleation event, but that it, in fact, occurs in regions in which the resolved shear stress is relatively small [8]. A second class of criteria associate the nucleation event to a buckling or phonon instability of the lattice (the Hill or Λ criteria based on mechanical stability arguments [7, 16]). MD simulations and experiments in different crystal indentation configurations, however, have revealed very complex nucleation processes in which the lattice is locally quite distorted, and therefore far from the conditions of applicability of the stability analyses. Large regions of partial dislocations and extended stacking faults have been argued to be present at nucleation [9], as well as extended and complex networks involving surfaces and grain boundaries [11]. The stability analysis of an undefected lattice has been recently reformulated away from the consideration of a mechanical phonon stability to the stability of the kinematic equation that governs the evolution of the dislocation density tensor. This approach is sensitive to the creation of non trivial local topology [8]. The predictions of this analysis are qualitatively different than the Schmid criterion.

The phase field crystal (PFC) model is a mesoscale description of a crystalline solid in which vibrational degrees of freedom have been averaged out, in the same spirit as density functional theory [13, 19]. The crystalline phase is described by a scalar order parameter field $\psi(\mathbf{r})$, which obeys a phenomenological free energy of the form

$$\mathcal{F}[\psi] = \int d\mathbf{r} \left[\frac{1}{2} [\mathcal{L}\psi]^2 + \frac{r}{2} \psi^2 + \frac{1}{4} \psi^4 \right], \quad (1)$$

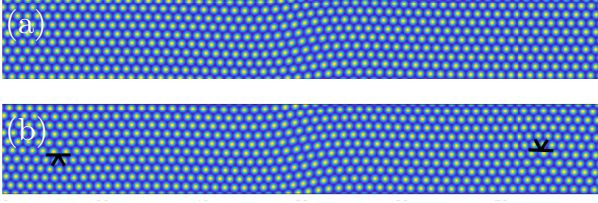


FIG. 1. Central region of the computational domain with (a), PFC configuration in equilibrium at $\sigma_0 = 0.080$ prior to nucleation, and (b), the equilibrium configuration at $\sigma_0 = 0.081$ after nucleation.

where $\mathcal{L} = 1 + \nabla^2$, and r is a dimensionless parameter representing the deviation from the liquid-solid phase boundary. We assume that ψ is a conserved variable with its spatial average $\bar{\psi}$ being constant [19]. In 2D, for a range of values of ψ and for $r < 0$, a triangular Bravais lattice $\psi^{eq}(\mathbf{r})$ is the equilibrium phase, which we consider here. Upon deformation of the equilibrium state ψ^{eq} by a displacement field $\mathbf{u}(\mathbf{x})$, the stress tensor can be directly obtained from the ψ in the deformed state as $\sigma_{ij}^\psi = \langle \tilde{\sigma}_{ij}^\psi \rangle$ [20], where $\langle \cdot \rangle$ refers to averaging over an area approximately equal to a unit lattice cell, and

$$\tilde{\sigma}_{ij}^\psi = -\partial_m[\psi \partial_m \mathcal{L} \psi] \delta_{ij} + 2[\partial_i \mathcal{L} \psi][\partial_j \psi], \quad (2)$$

where $X_{(i}Y_{j)}$ refers to the symmetrization of indices i, j [21]. In linear elasticity, a hexagonal lattice is isotropic. Hence the strain is

$$e_{ij}^\psi = \frac{1}{2\mu}(\sigma_{ij}^\psi - \kappa \delta_{ij} \sigma_{kk}^\psi). \quad (3)$$

where μ is the shear modulus, and $\kappa = \lambda/(2(\lambda + \mu))$, where λ is the standard Lamé coefficient. These elastic constants can all be related to the amplitude of the equilibrium state ψ^{eq} [22]. Dislocations lead to lattice incompatibility [4, 23]. In 2D, and given a Burgers vector density $\mathbf{B}(\mathbf{r})$, the incompatibility field is $\eta = \epsilon_{ik}\epsilon_{jl}\partial_{ij}e_{kl} = \epsilon_{ij}\partial_i B_j$. A key assumption is that the configuration of ψ contains the complete strain incompatibility [22, 24]. Thus, taking the incompatibility of Eq. (3) we define

$$\eta^\psi = \frac{1}{2\mu}(\epsilon_{ik}\epsilon_{jl}\partial_{ij}\sigma_{kl}^\psi - \kappa \nabla^2 \sigma_{kk}^\psi). \quad (4)$$

The dissipative evolution of ψ is diffusive $\partial_t \psi = \nabla^2 \frac{\delta \mathcal{F}}{\delta \psi}$, with constant mobility (set to one in dimensionless units). As discussed in Ref. [22], lattice distortion needs to be treated separately from diffusive relaxation of ψ in order to maintain elastic equilibrium at all times. In order to induce nucleation, we consider an externally imposed bulk stress $\sigma_{ij}^{ext}(\mathbf{r})$. In elastic equilibrium $\partial_i \sigma_{ij}^\psi = \partial_i \sigma_{ij}^{ext}$. Following Ref. [22], for a nonequilibrium configuration of ψ , we solve $\partial_i(\sigma_{ij}^\psi - \sigma_{ij}^{ext} + \sigma_{ij}^\delta) = 0$, where $\sigma_{ij}^\delta = \lambda e_{kk}^\delta + 2\mu e_{ij}^\delta$, and e_{ij}^δ is a compatible strain $e_{ij}^\delta = (\partial_i u_j^\delta + \partial_j u_i^\delta)/2$. Diffusion of ψ is supplemented at

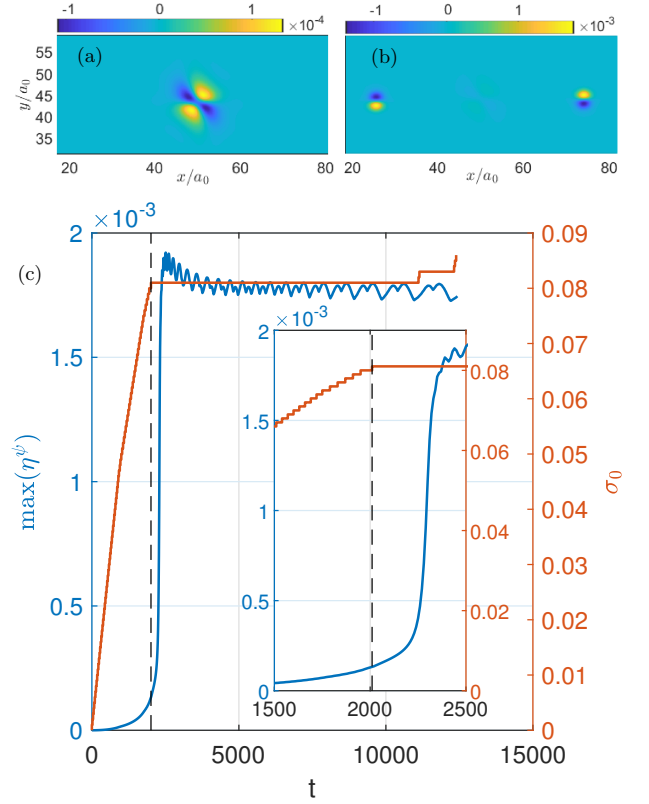


FIG. 2. a) Incompatibility field η^ψ (a) at $t = 2050$ ($\sigma_0 = 0.080$), before the nucleation event, and (b) at $t = 12170$ ($\sigma_0 = 0.081$) after nucleation. c) Maximum of η^ψ as a function of time t . Nucleation takes place at $t \approx 2300$. The right axis shows the value of σ_0 for the corresponding times. The plateaus in time indicate non-equilibrium relaxation at constant external stress.

each time by distortion $\psi(\mathbf{r}) \rightarrow \psi(\mathbf{r} - \mathbf{u}^\delta)$. In 2D, the condition for elastic equilibrium means that the stress tensor difference can be written in terms of an Airy potential χ , $\sigma_{ij}^\psi - \sigma_{ij}^{ext} + \sigma_{ij}^\delta = \epsilon_{ik}\epsilon_{jl}\partial_{kl}\chi$. For each instantaneous configuration of ψ we solve [22],

$$\frac{1 - \kappa}{2\mu} \nabla^4 \chi = \eta^\psi - \eta^{ext}, \quad (5)$$

where η^{ext} accounts for the fact that the imposed stress does not necessarily derive from a compatible strain. The solution allows the computation of e_{ij}^δ and, from it, of the displacement u_i^δ .

We impose a shear stress $\sigma_{xx}^{ext} = \sigma_{yy}^{ext} = 0$ and $\sigma_{xy}^{ext} = \sigma_0 e^{-\frac{|\mathbf{r} - \mathbf{r}_0|^2}{2w^2}}$, with \mathbf{r}_0 an arbitrary center. A square computational domain is considered with 100×100 hexagonal unit cells of length $a_0 = \frac{4\pi}{\sqrt{3}}$ with grid spacings $\Delta x = a_0/7$ and $\Delta y = a_0\sqrt{3}/12$. Model parameters are $r = -1$ and $\bar{\psi} = -0.45$. The initial condition of ψ is a periodic, hexagonal lattice, with the corresponding Lamé coefficients $\mu = \lambda = 0.227$. In order to study nucleation, we define the following protocol: the diffusion equation for

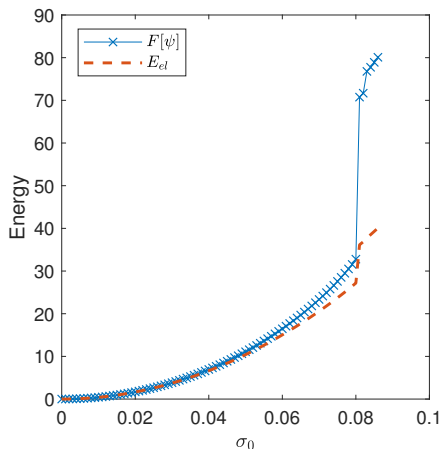


FIG. 3. Total free energy \mathcal{F} and elastic energy E_{el} as function of σ_0 .

ψ is propagated in time for 100 time steps by using an exponential time differencing method with a time step of $\Delta t = 0.1$ [25], after which ψ is brought to mechanical equilibrium by the compatible distortion [22, 26]. Once the maximal difference of ψ between two such protocol iterations is less than 0.01, we increase σ_0 by an increment $\Delta\sigma_0 = 0.001$ and stop the simulation at $\sigma_0 = 0.086$. Figure 1 shows the equilibrated field ψ prior to and after a nucleation event for $w = 4a_0$ and $\sigma_0 = 0.080$ and 0.081 .

The nucleation event can be clearly observed in the incompatibility field η^ψ . Figures 2(a) and 2(b) show this field for the same equilibrated configurations of Fig. 1. The extremes in the value of η^ψ identify the location of the defect cores. Also, the quadrupolar structure of Fig. 2(a) *prior* nucleation reflects the Burgers vectors of the dislocation pair to be nucleated. More quantitatively, Fig. 2(c) shows the evolution of the maximal value of η^ψ upon increasing σ_0 . The observed nucleation point is marked by the vertical dashed line. We observe that $\max(\eta^\psi)$ rises before the actual nucleation event.

Figure 3 further shows the corresponding change in the PFC free energy \mathcal{F} upon increasing σ_0 , together with the elastic energy defined as $E_{el} = \frac{1}{2} \int d\mathbf{r} \sigma_{ij}^\psi e_{ij}^\psi$. Note that despite the purely diffusive dynamics obeyed by ψ , the lattice is capable of storing (reversible) elastic energy upon increasing the value of σ_0 , as it should. This reversible evolution is enabled through the compatible distortion added to the field ψ to preserve elastic equilibrium. As the nucleation event is reached, the phase field energy exhibits a large discontinuity at the same value of σ_0 that corresponds to the dashed line in Fig. 2(c).

It is possible to predict the nucleation event from the value of the resolved shear stress along each slip plane, in analogy with the classical Schmidt criterion. For a given stress σ_{ij} , the resolved shear stress $\tau_{\mathbf{a},\mathbf{n}}$ on a slip plane defined by the normal unit vector \mathbf{n} along a direction in the slip plane given by the unit vector \mathbf{a} is $\tau_{\mathbf{a},\mathbf{n}} = a_i \sigma_{ij} n_j$. In 2D, \mathbf{n} is determined up to a sign by $n_i = \epsilon_{ij} a_j$, and

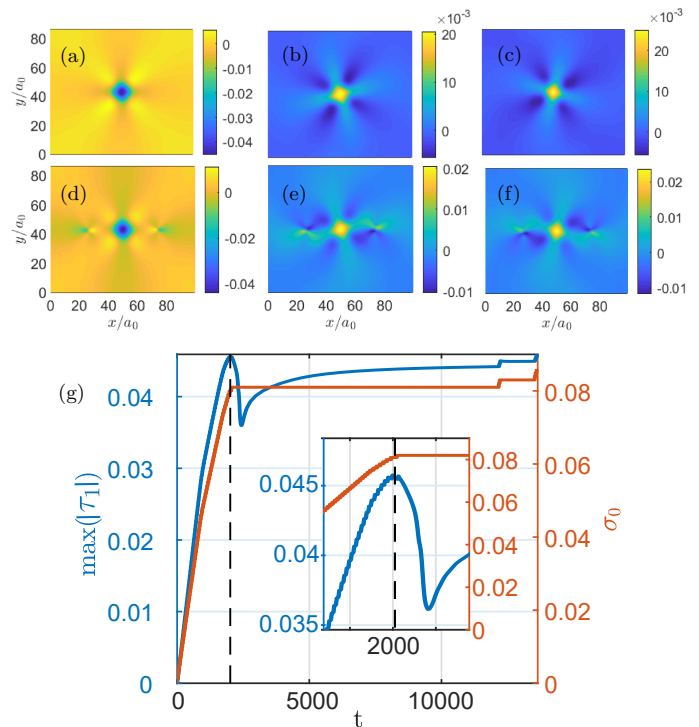


FIG. 4. The resolved shear stresses just prior to and after the nucleation event. (a-c) τ_1 , τ_2 , τ_3 at $t = 2050$ ($\sigma_0 = 0.080$), respectively, (d-f) τ_1 , τ_2 , τ_3 at $t = 12170$ ($\sigma_0 = 0.081$), respectively. (g) $\max(|\tau_1|)$ as function of time t during the nucleation event.

for the hexagonal symmetry, there are three slip planes defined by lattice vectors $\mathbf{a}_1 = [1, 0]$, $\mathbf{a}_2 = [1/2, \sqrt{3}/2]$, and $\mathbf{a}_3 = [-1/2, \sqrt{3}/2]$. One thus considers three different scalar fields τ_1 , τ_2 , and τ_3 , which are the resolved shear stresses along the slip directions corresponding to \mathbf{a}_1 , \mathbf{a}_2 and \mathbf{a}_3 , respectively. Figures 4(a-f) show the fields τ_1 , τ_2 , τ_3 right before and after nucleation. The resolved shear stress is largest along the \mathbf{a}_1 direction, the slip plane along which the dislocation pair nucleates, and is centered at the origin, the nucleation site. The other two resolved stresses remain small during nucleation. The evolution in time of the largest resolved stress τ_1 is shown in Fig. 4(g). Nucleation occurs (vertical dashed line in the figure) when the resolved shear stress approaches the critical value of $|\tau_c| = 0.046$, followed by a small drop, and then a slow rise as the newly nucleated dislocation dipole moves away from the center region. Notice that this value of τ_c at the moment of nucleation is smaller than the external shear stress $\sigma_{xy}^{ext} = 0.080$. This is because at mechanical equilibrium, the two stresses are equal only up to a divergence-free term. The critical value of the resolved stress τ_c can be estimated as follows: Consider an otherwise perfect lattice with a bound dislocation pair of opposite Burgers vectors. The force acting on the dislocations (in opposite directions) because of the external stress is the Peach-Koehler force projected on the slip plane defined by \mathbf{a}_k , and is $F_k^{PK} = b\tau_k = \pm a_0\tau_k$, for

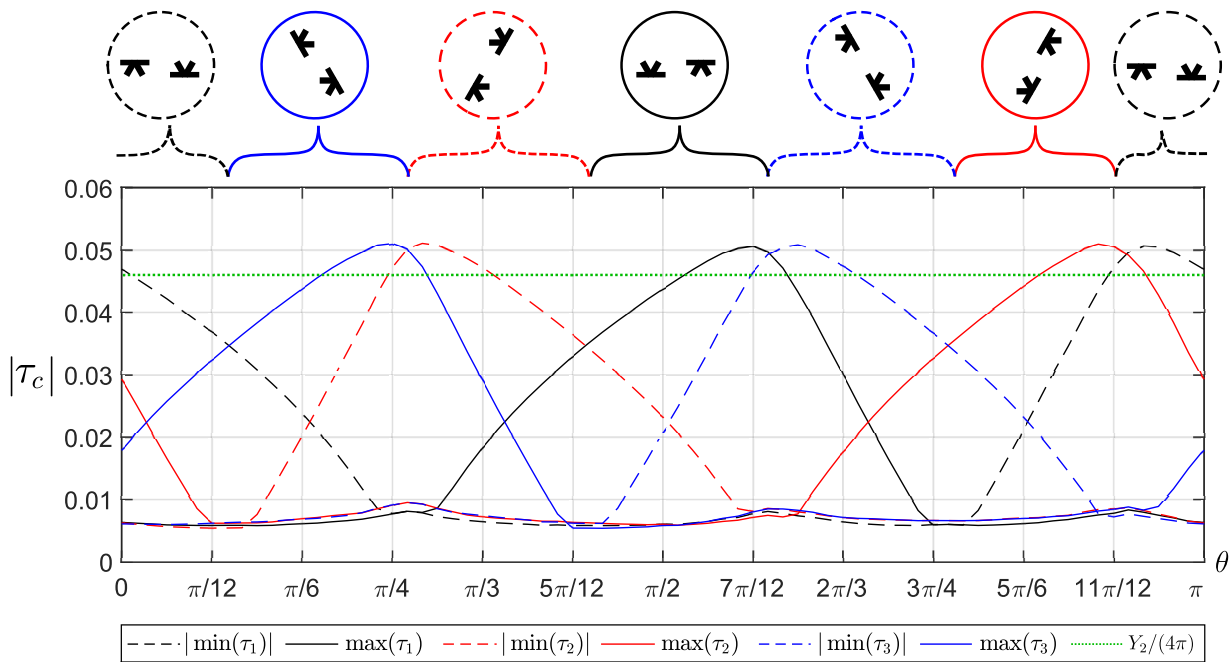


FIG. 5. (Color online) The critical value of $|\tau_c|$ as a function of the rotation angle θ of the externally imposed stress $\sigma_{ij}^{ext}(\theta)$. The top row shows the type of dislocation dipole that nucleates and the resolved stress along the slip plane with the largest value that determines the type of dislocation dipole to nucleate.

dislocations with Burgers vectors $\mathbf{b} = \pm a_0 \mathbf{a}_k$. As the two dislocations in the dipole separate at nucleation to become distinct, their mutual elastic interaction results in an attractive force. If both dislocations are on the x axis, this force is [27, 28] $|f_x| = Y_2 b^2 / (4\pi d)$, where $Y_2 = 4\mu(\lambda + \mu) / (\lambda + 2\mu)$ is the 2D Young modulus, and d the dislocation separation. We estimate τ_c as the applied stress for which the resulting Peach-Koehler force on one dislocation equals the force from the other dislocation when the separation is one lattice constant. We find that $\tau_c = Y_2 / (4\pi)$. Using the numerical values of $\mu = \lambda = 0.2271$, $Y_2 / (4\pi) = 0.048$, which is in close agreement with the observed value of $|\tau_c| = 0.046$.

To further test the nucleation criterion, we have performed additional calculations in which the imposed stress σ_{ij}^{ext} is rotated relative to the lattice, $\sigma_{ij}^{ext}(\theta) = R_{ki}^{(\theta)} \sigma_{kl}^{ext} R_{lj}^{(\theta)}$, where $R_{ij}^{(\theta)}$ is the standard rotation matrix in 2D, and θ is the rotation angle. Figure 5 shows the maximal resolved stress along the three lattice directions as a function of θ . Since σ_{ij}^{ext} is invariant under a rotation of π , $\sigma_{ij}^{ext}(x) = \sigma_{ij}^{ext}(\pi + x)$, we show only values ranging from $\theta = 0$ to π . The figure shows that the resolved stress consistently predicts the type of dislocation dipole to nucleate, but the value of the critical resolved stress depends on θ , and is in general lower than $Y_2 / (4\pi)$. The discrepancy is likely due to anisotropic contributions to lattice distortions at the length scale of the core which are not described by isotropic linear elasticity.

To conclude, we have shown that the incompatibility field η^ψ is very sensitive to the nucleation of a dislocation dipole, and that it signals the nucleation event prior to

the formation of a stable topological dipole. The symmetry of the field η^ψ prior to nucleation also gives the direction of the Burgers vectors of the defect pair about to nucleate. By examining the distribution of the resolved stress for a hexagonal lattice, we have also found it to be a good indicator of nucleation. Furthermore, a balance between the Peach-Koehler force on either one of the defects of the dipole and their mutual elastic interaction force allows a prediction of the resolved stress at nucleation that agrees well with the numerical results. While our results serve to extend those of macroscopic plasticity by allowing the direct observation of the incompatibility field and its evolution under an applied stress, the conclusion that a Schmid like criterion identifies the nucleation event appears to be in disagreement with several MD simulations in the prototypical configuration involved in nanoindentation studies. These MD simulations show that the resolved stress does not predict the location nor type of dislocations to nucleate. Instead, it is generally observed that the nominal extent of the nucleation region is very large, with a complex network of stacking faults, partial dislocations, and other significant sources of lattice distortion. These results would imply that the nucleation path in configuration space is very complex, with possibly multiple competing trajectories that depend on details such as boundaries or applied stress protocols. Given such a complexity of detail, it is also unclear how suitable the interatomic potentials used in the simulations are to describe the observed large and localized distortions at very high stresses used (GPa). We have shown that the PFC provides adequate con-

trol over configurations and applied stresses, and hence is a suitable platform for testing nucleation criteria. The model also offers the necessary separation between length scales, eliminates fluctuations of thermal origin, and allows the computation of internally generated stress that contribute to lattice incompatibility, and ultimately to nucleation.

ACKNOWLEDGMENTS

We thank Amit Acharya, Kristian Olsen and Jonas Rønning for many stimulating discussions. The research of J.V. has been supported by the National Science Foundation, Grant No. DMR-1838977. L.A. acknowledges support from the Kavli Institute for Theoretical Physics through the National Science Foundation under Grant No. NSF PHY-1748958.

-
- [1] J. S. Langer, *Ann. Phys.* **54**, 258 (1969).
 - [2] J. Gunton, M. San Miguel, and P. Sahni, *Kinetics of first order phase transitions*, edited by C. Domb and J. Lebowitz, Phase Transitions and Critical Phenomena, Vol. 8 (Academic, London, 1983).
 - [3] A.-C. Davis and R. H. Brandenberger, *Formation and interactions of topological defects*, NATO ASI, Vol. B 349 (Plenum Pub. Corp., 1995).
 - [4] J. Friedel, “Dislocations - an introduction,” in *Dislocations in solids, vol. 1*, edited by F. R. N. Nabarro (North-Holland Publishing Company, 1979) p. 1–32.
 - [5] R. Phillips, *Crystals, defects and microstructures: modeling across scales* (Cambridge University Press, 2001).
 - [6] J. Li, K. J. Van Vliet, T. Zhu, S. Yip, and S. Suresh, *Nature* **418**, 307 (2002).
 - [7] R. E. Miller and A. Acharya, *Journal of the Mechanics and Physics of Solids* **52**, 1507 (2004).
 - [8] A. Garg, A. Acharya, and C. E. Maloney, *Journal of the Mechanics and Physics of Solids* **75**, 76 (2015).
 - [9] C. L. Kelchner, S. J. Plimpton, and J. C. Hamilton, *Phys. Rev. B* **58**, 11085 (1998).
 - [10] T. Zhu, J. Li, A. Samanta, A. Leach, and K. Gall, *Phys. Rev. Lett.* **100**, 025502 (2008).
 - [11] X. Li, Y. Wei, L. Lu, K. Lu, and H. Gao, *Nature* **464**, 877 (2010).
 - [12] K. R. Elder, M. Katakowski, M. Haataja, and M. Grant, *Phys. Rev. Lett.* **88**, 245701 (2002).
 - [13] H. Emmerich, H. Löwen, R. Wittkowski, T. Gruhn, G. Tóth, G. Tegze, and L. Gránásy, *Adv. Phys.* **61**, 665 (2012).
 - [14] J. R. Rice, *Journal of the Mechanics and Physics of Solids* **40**, 239 (1992).
 - [15] J. Li, T. Zhu, S. Yip, K. J. Van Vliet, and S. Suresh, *Materials Science and Engineering: A* **365**, 25 (2004).
 - [16] R. E. Miller and D. Rodney, *Journal of the Mechanics and Physics of Solids* **56**, 1203 (2008).
 - [17] A. Garg and C. E. Maloney, *Journal of Applied Mechanics* **83** (2016).
 - [18] M. Duesbery and V. Vitek, *Acta Mater.* **46**, 1481 (1998).
 - [19] K. R. Elder, N. Provatas, J. Berry, P. Stefanovic, and M. Grant, *Physical Review B* **75**, 064107 (2007).
 - [20] A. Skaugen, L. Angheluta, and J. Viñals, *Physical Review B* **97**, 054113 (2018).
 - [21] This version of the microscopic stress tensor is slightly different than in [20], but it has the same divergence. Therefore they are physically equivalent.
 - [22] A. Skaugen, L. Angheluta, and J. Viñals, *Phys. Rev. Lett.* **121**, 255501 (2018).
 - [23] E. Kröner, *Physics of Defects*, edited by R. B. et al., Les Houches, Session XXXV (North-Holland, Amsterdam, 1981).
 - [24] A. Acharya and J. Viñals, *Phys. Rev. B* **102**, 064109 (2020).
 - [25] S. M. Cox and P. C. Matthews, *Journal of Computational Physics* **176**, 430 (2002).
 - [26] M. Salvalaglio, L. Angheluta, Z.-F. Huang, A. Voigt, K. R. Elder, and J. Viñals, *Journal of the Mechanics and Physics of Solids* **137**, 103856 (2020).
 - [27] P. M. Chaikin and T. C. Lubensky, *Principles of Condensed Matter Physics* (Cambridge University Press, 1995).
 - [28] B. Perreault, J. Viñals, and J. M. Rickman, *Phys. Rev. B* **93**, 014107 (2016).